A Similarity Criterion of the Optimal Process in Melt Spinning

Y. D. KWON, R. H. BUTLER, and D. C. PREVORSEK, *Corporate Research Center, Allied Chemical Corporation, Morristown, New Jersey 07960*

Synopsis

Experimental and simulation studies of optimization of the melt spinning process were carried out for nylon 6 fibers. The experiment and process simulation demonstrated that one criterion that can be applied in scaling up an optimized melt spinning process is to achieve the similar real time history of temperature and deformation rate in the spinway. Some aspects of the experiments and process simulation are discussed, together with the results of real time history analysis for a case of nylon 6 spinning.

INTRODUCTION

In industrial applications, the most important problems of melt spinning are: (1) the optimization of the process with respect to a given fiber property, a set of properties, a set of properties coupled with some other factors, such as production rate, quality of the final product, product uniformity, etc.; (2) the transfer of an optimized process from one type of equipment to some other type; and (3) the modifications of an optimized process to account for changes in product specifications, alterations in the spinway, etc.

The present understanding of melt spinning and drawing processes is, in most cases, insufficient to predict without extensive experimentation the optimum conditions for a given product. As a rule, these goals are achieved by various types of experimental work.

The transfer of an optimized process from one type of equipment to another on one hand and the modifications in the process to account for changes in production rate, alterations in equipment design, etc. on the other hand can be greatly facilitated by means of modern computational and simulation techniques.

In this article we describe a method that is suitable to solve the problems described above. The principle of the method is based on the assumption that the properties of the fiber are uniquely defined by its temperature and deformation rate history. The mathematical problem is, therefore, to establish the changes in operational variables to match the temperature and deformation rate history of the filaments when equipment design or production rates are changed.

THEORY

Experimental and analytical studies of the melt spinning process have been carried out by many authors. Most of the studies were concerned with the rheological and heat transfer aspects of the melt spinning process.[1–5] Recently, some authors investigated the change of fiber structure in the spinway by use

Journal of Applied Polymer Science, Vol. 25, 1165–1178 (1980)

0021-8995/80/0025-1165$01.40

of x-ray and birefringence devices.[6,7] The findings from these studies help to understand the dynamics of filament thinning, filament quenching, and change of fiber structure in the melt spinning process.

Referring to Figure 1, which depicts the schematics of a melt spinning process, let us consider a small particle of the fiber material leaving the spinneret at $t = 0$ (t denoting the real time) and traveling down the spinway toward the take-up roll while being subjected to a certain conditioning history. For simplicity, we assume that at a position z (or time t), condition of the fiber material is uniform across the radius of filament. In other words, we disregard the distributed nature of the system and treat it as a lumped parameter system. Suppose that the state of fiber material can be described completely by n state variables of $x_1, x_2, \ldots x_n$ (or $\mathbf{x}$ in shorthand notation) which vary with time by the dynamic relation of

$$\frac{dx_i}{dt} = f_i(x_1, x_2 \ldots x_n, u_1, u_2 \ldots u_m) \tag{1}$$

where u_i indicates the process control variables. If the objective function J (the tensile strength, for example) to be optimized can be expressed by

$$J = F(\mathbf{x}(t_f)) + \int_0^{t_f} L(\mathbf{x},\mathbf{u})dt \tag{2}$$

then the problem of optimizing the melt spinning process to achieve a desired optimal value of J is mainly that of a numerical computation based on the mathematical principles of optimization.

The real problem we face in spinning process analysis, like in many other physical processes, is that we do not have complete knowledge of the relations,

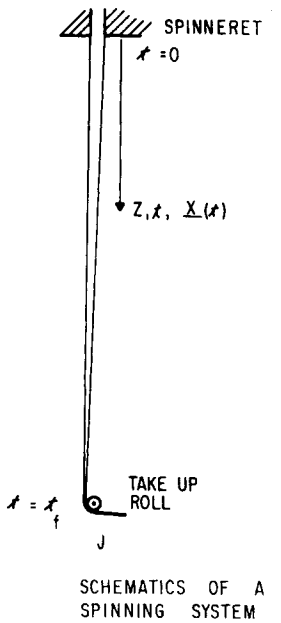

Fig. 1. Schematics of a spinning system. z = position; t = time; $\mathbf{x}$ = state variables; J = objective function.

such as eqs. (1) and (2). Thus, the only available way of optimizing the melting spinning process is experimentation.

After an optimal process is established by experimental procedure, it is often desirable to scale up the process while achieving the same objective. Again, owing to the lack of knowledge of the relations of eqs. (1) and (2), the scale-up work necessitates an experimental optimization. In this case, however, if the real time history of the state variables, $\mathbf{x}(t)$, is known for the first process, then the second process, i.e., the scaled-up process, can be expected to yield a same value of the objective function J if the history of $\mathbf{x}(t)$ is somehow kept the same. This is so although we do not know the relation of eq. (2). In other words, between process 1 and process 2, if

$$\mathbf{x}_1(t) = \mathbf{x}_2(t) \quad \text{for } t = 0 \sim t_f \tag{3a}$$

then we can expect

$$J_1 = J_2 \tag{3b}$$

Thus, scale-up of an optimal process can be achieved by achieving the similarity of the history of state variables.

For the above-mentioned simplified lumped parameter system of a melt spinning process, we consider the filament temperature $T(t)$ and the rate of filament thinning $dV(t)/dz$ as the two state variables of the system which affect predominantly the changes in properties of the fiber during spinning. Denoting the temperature history and the thinning rate history of the filament in the first optimized melt spinning process by $T_1(t)$ and $dV_1(t)/dz$, respectively, and those of the second scaled-up process by $T_2(t)$ and $dV_2(t)/dz$ for $t = 0 - t_f$, we hypothesize that, if

$$T_1(t) = T_2(t) \tag{4a}$$

and

$$dV_1(t)/dz = dV_2(t)/dz \tag{4b}$$

then

$$J_1 = J_2$$

The idea underlying this hypothesis is that as long as the temperature history and deformation rate history of a fiber material starting from the same initial state are the same, the changes in the material characteristics, such as molecular weight distribution and morphology, should also be the same.

Now, let us examine whether it is possible to achieve the relations of (4a) and (4b) in a melt spinning process, and if it is, then under what condition. Referring to Figure 2, in which two spinning processes are compared, let w, H, D, and V denote the mass rate of spinning material, height of the spinway, filament diameter, and filament velocity, respectively, and let the numeral subscripts 1 and 2 refer to processes 1 and 2. The position variable z is related to the velocity V by

$$dz = V\,dt \tag{5}$$

Therefore,

$$\frac{dV}{dz} = \frac{1}{V}\frac{dV}{dt} = \frac{d \ln V}{dt} \tag{6a}$$

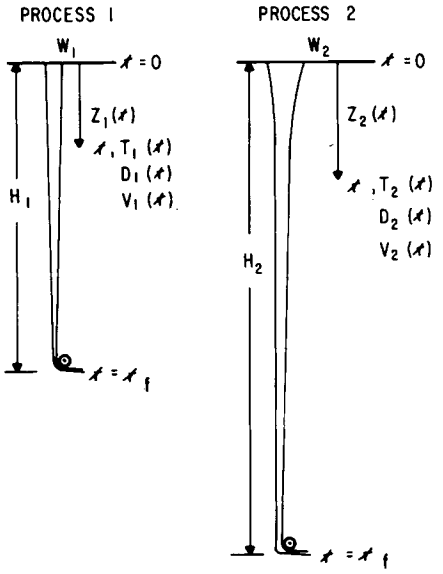

Fig. 2. Two spinning processes.

So, the relation of eq. (4b) dictates

$$V_1(t)/V_1(0) = V_2(t)/V_2(0) = s(t) \tag{6b}$$

which means that the stretch ratio based on the initial filament velocity, $s(t)$, is the same between process 1 and process 2.

If we set the scale-up factors for the mass rate and the filament diameter to take-up to c and r, respectively,

$$w_2 = cw_1 \tag{7}$$

and

$$D_{2_f} = rD_{1_f} \tag{8}$$

where the subscript f indicates the final take-up point in the spinway. The mass balance at the take-up point requires

$$V_{2_f} = (c/r^2)V_{1_f} \tag{9}$$

and eq. (6b) extends eq. (9) to

$$V_2(t) = (c/r^2)V_1(t) \tag{10a}$$

$$V_2(0) = (c/r^2)V_1(0) \tag{10b}$$

$$D_2(t) = rD_1(t) \tag{10c}$$

The spinway height H is given by

$$H = \int_0^{t_f} V(t)dt = V(0) \int_0^{t_f} s(t)dt$$

$$H_2/H_1 = V_2(0)/V_1(0) = c/r^2 \tag{11}$$

The equality relations of (4a) and (4b) require the equality of the elongational stress $\sigma(t)$ between processes 1 and 2. Under the one-dimensional elongation, $\sigma(t)$ is given by

$$\sigma(t) = \eta_T[dV(t)/dz] \tag{12}$$

where η_T is the tensile viscosity. Tensile viscosity has been found to be a function of the temperature only[8] or to be a function of temperature and elongation rate, dV/dz.[9] In either case, eqs. (4a) and (4b) would result in

$$\eta_{T_1}(t) = \eta_{T_2}(t) \tag{13}$$

and

$$\sigma_1(t) = \sigma_2(t) \tag{14}$$

The "rheological force" F_{rheo} has been defined conventionally by

$$F_{\text{rheo}}(t) = \sigma(t) \times 0.785[D(t)]^2 \tag{15}$$

In view of eqs. (10c) and (14), we have

$$F_{\text{rheo }2}(t) = r^2 F_{\text{rheo }1}(t) \tag{16}$$

Equations (6)–(16) are the relations which would result if the requirements of eqs. (4a) and (4b) were fulfilled. Now, we have to ask under what conditions these requirements can be realized.

Obviously, the first requirement is the controllability of filament temperature $T(t)$ for achieving $T_2(t) = T_1(t)$. Equation (4a) implies

$$dT_1(t)/dt = dT_2(t)/dt \tag{17}$$

For the simplified one-dimensional system, dynamics of the filament quenching can be approximated by

$$\rho C_p(0.785D^2)dz(dT/dt) = -3.14D\,dz\,h_c(T - T_a) - 3.14D\,dz\,h_r(T_k{}^4 - T_{sk}{}^4) \tag{18}$$

where ρ, C_p, h_c, h_r, and T_a represent the density of fiber, heat capacity of fiber, convective heat transfer coefficient, radiative heat transfer coefficient, and the ambient air temperature. T_k and T_{sk} denote the filament temperature and spinway wall temperature in the Kelvin scale. Equation (18) simplifies to

$$dT/dt = (-4/\rho C_p D)h_c(T - T_a) - (4/\rho C_p D)h_r(T_k{}^4 - T_{sk}{}^4) \tag{19}$$

Equation (17) necessitates the relation

$$\frac{h_{c_1}(t)}{D_1(t)}[T_1(t) - T_{a_1}(t)] + \frac{h_{r_1}(t)}{D_1(t)}[(T_{k_1}(t))^4 - (T_{sk_1(t)})^4] = \frac{h_{c_2}(t)}{D_2(t)}[T_2(t) - T_{a_2}(t)] + \frac{h_{r_2}(t)}{D_2(t)}[(T_{k_2}(t))^4 - (T_{sk_2}(t))^4] \tag{20}$$

Thus, there are four variables that can be manipulated in eq. (20) to achieve the equality of eq. (17): h_c, h_r, T_a, and T_{sk}.

Consider a case, for example, in which $D_1(t) = D_2(t)$ but the speed of filament is increased by a factor of 2. When the quench air and filament flow in parallel direction, the convective heat transfer coefficient h_c is correlated to air flow condition by Muller's correlation,[10] i.e.,

$$h_c D/k_a = 0.42(VD\rho_a/\mu_a)^{0.33} \tag{21}$$

where k_a, ρ_a, and μ_a denote the thermal conductivity, density, and viscosity of

air, respectively. Thus, increase of V raises the value of h_c; and in order to maintain the equality of eq. (2), it is necessary to raise $T_{a_2}(t)$ and/or $T_{sk_2}(t)$ to offset the effect. One means of providing the variation of T_{sk} is the heated sleeves surrounding the spinway.

In this way, the controllability of filament temperature hinges on whether the equality of eq. (20) can be maintained by the manipulation of the above-said four variables within the allowable and attainable ranges. However, it is physically impossible to manipulate these variables from point to point. Practically, the only feasible way of manipulating these variables is to do so by segments of finite lengths. Therefore, in a rigorous sense, the control can be achieved only approximately. Experimental runs to be described later have shown, however, that the actual controllability of temperature in the scale-up of a moderate ratio is fairly good.

After the temperature controllability, another controllability problem is related to the rheological force, F_{rheo}, given by eq. (15). Denoting the take-up tension by F_T, F_{rheo} at position z in a spinway of height H can be approximated by

$$F_{\text{rheo}}(z) = F_T + \int_z^H \rho g \pi D^2 \, dz/4 - \int_z^H \tau \pi D \, dz - w[V_f - V(z)] \quad (22)$$

where g is the gravity constant and τ is the skin friction at filament surface owing to the air drag. Thus, the second, third, and fourth terms on the right-hand side are for the filament weight effect, air drag effect, and inertia effect on the filament tension, respectively.

Equations (14) and (15) necessitate the relation

$$F_{\text{rheo}_1}(t)/[D_1(t)]^2 = F_{\text{rheo}_2}(t)/[D_2(t)]^2$$

or

$$r^2 F_{\text{rheo}_1(t)} = F_{\text{rheo}_2}(t) \quad (23)$$

If in eq. (22) $F_{\text{rheo}}(z) = F_T$, that is, the total sum of the effects of gravity, air drag, and inertia is negligible relative to F_T, then it can be shown* that eq. (23) holds by itself once the temperature is controllable. When this is not the case, eqs. (22) and (23) require

$$r^2 \left[\int_{z_1(t)}^H \rho g \frac{\pi D_1^2}{4} dz_1 - \int_{z_1(t)}^H \tau_1 \pi D_1 \, dz_1 - w_1[V_{1f} - V_1(z_1)] \right.$$
$$= \int_{z_2(t)}^{H_2} \rho g \frac{\pi D_2^2}{4} dz_2 - \int_{z_2(t)}^{H_2} \tau_2 \pi D_2 \, dz_2 - w_2[V_{2f} - V_2(z_2)] \quad (24)$$

Equality of eq. (24) is achieved to a good approximation if

$$c = r^2 \quad (25)$$

which means, resulting from eq. (9),

$$V_1(t) = V_2(t) \quad (26)$$

Otherwise the equality does not hold strictly and the requirement for eq. (23) cannot be held rigorously. However, as shown by the experimental results, the

* $r^2 F_{\text{rheo}_1}(t) = r^2, \ \eta_{T_1}(t) \frac{dV_1}{dz}(t) \frac{\pi[D_1(t)]^2}{4} = \eta_{T_2}(t) \frac{dV_2}{dz}(t) \frac{\pi[D_2(t)]^2}{4} = F_{\text{rheo}_2}(t).$

equality can be maintained approximately when the scale-up ratio is moderate.

In order to minimize the deviations between $T_1(t)$, $dV_1(t)/dz$, and $T_2(t)$, $dV_2(t)/dz$, one can use the Pontryagin's minimum principle[11] to minimize the deviation function:

$$\Delta = \int_0^{t_f} [(T_1(t) - T_2(t)]^2 + \beta \left(\frac{dV_1(t)}{dz} - \frac{dV_2(t)}{dz}\right)^2 dt \qquad (27)^{**}$$

by optimal selection of $T_a(t)$, $T_{sk}(t)$, and $V_a(t)$, where $V_a(t)$ is the quench air velocity which affects the convective heat transfer coefficient h_c and the skin friction owing to air drag, τ. Details of this numerical procedure will be described elsewhere. Here, it is sufficient to say that the result of this procedure provides the guidance for varying the values of T_a, T_{sk}, and V_a as the function of the position.

EXPERIMENTAL

Schematics of the experimental spinning system is shown in Figure 3. It is similar to an ordinary melt spinning system with the spinneret die at top and the take-up roll at the bottom. The special feature of this spinning system is the series of sleeves which are stacked in vertical direction, surrounding the spinway. The individual sleeve had an internal diameter of 10 cm (4 in.) and a length of 15 cm (6 in.), and the sidewall is wrapped with heating band and in-

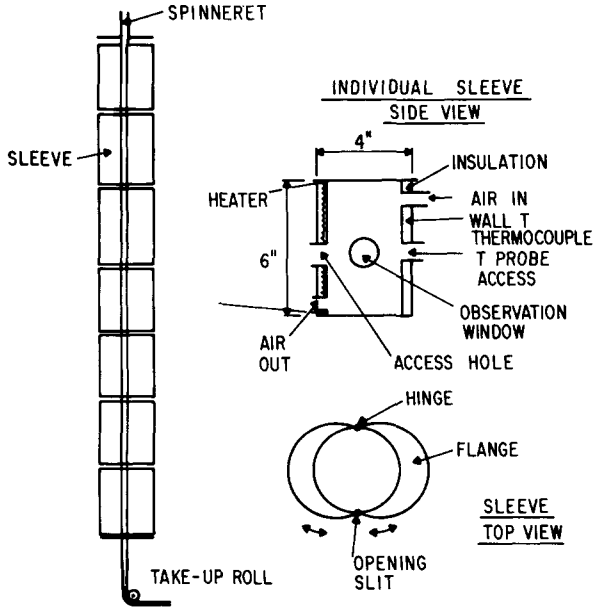

Fig. 3. Schematics of experimental spinning system.

** Δ indicates the magnitude of deviations of $T_2(t)$ and $dV_2/dz(t)$ from $T_1(t)$ and $dV_1/dz(t)$. β is a scale factor, and its numerical value is chosen such that $[T_1(t) - T_2(t)]^2$ and $[dV_1/dz - dV_2/dz]^2$ are of comparable magnitudes numerically.

sulation materials. The sleeve is made of two halves of a cylinder which are combined by the hinge in order to facilitate opening the sleeve when necessary. The sidewall has five circular openings. The observation window at the front center is provided for observation of filament when the probe for filament temperature measurement is inserted through the temperature probe access hole and is brought into contact with the filament. The openings for the air inlet and air outlet are installed on individual sleeve to facilitate the variation of air temperature and air velocity locally. The additional access hole on the left-hand side was installed to allow illumination of the filament while photograph of the filament for the purpose of determining the filament diameter was taken by a camera through the front observation window. A thermocouple tip was placed on the inner wall of the sleeve to monitor the sleeve wall temperature. The air temperature inside the sleeve was measured by inserting a thermocouple through the temperature probe access hole, and the air velocity was measured by inserting an anemometer through the same access hole.

Using this spinning system, the experimental optimization of the process for maximizing the tensile strength of filament obtained by drawing after spinning was carried out as follows:

(1) After setting up the system, the extrusion was started at a prescribed rate with the melt at the spinning die fixed at a suitable temperature.

(2) The sleeve temperatures were set to an initial profile and the air flow was set to an initial pattern.

(3) Then, the filament was taken up by the take-up roll at an initial take-up speed.

(4) The spun yarn was drawn to a fixed draw ratio at a fixed set of conditions. The drawing conditions were fixed in this case because our study was focused at the optimal condition of the spinning with other conditions fixed.

(5) After the drawing, the tensile strength of the filament was measured.

(6) Then, sequentially, systematic variations were made of the take-up speed, sleeve temperatures, and air flow rate.

(7) The run which gave the maximum tensile strength was repeated, and at this time measurements were made of the filament temperature and filament diameter at each of the sleeves. The filament temperature was measured by the contact null-point device,[12] and the filament diameter was measured by close-up photography.

(8) The temperature and diameter data were interpolated by the digital simulation technique, which will be described in Appendix A.

Thus, by the experimental optimization and digital simulation for interpolating the experimentally measured temperature and diameter profiles, we could establish the complete profiles of temperature and diameter for an optimized spinning process.

Next, the extrusion rate was varied and then the same optimization experiment was repeated to achieve the maximum tensile strength of the filament. Again, from the experimental data, the optimal temperature profile and diameter profile were established by interpolating the data by the digital simulation technique. Then, the optimal profiles thus established were compared to each other to examine the similarity in the real time history of temperature and elongation rate in the spinway.

RESULTS AND DISCUSSION

Measurement and Simulation of Temperature and Diameter Profiles

Figure 4 shows an example of the temperature and diameter profiles measured and interpolation of the data by digital simulation. Nylon 6, 11 g/min, at 271°C (520°F) was extruded through a 20–0.0457-cm (18 mil) hole spinneret die and the yarn was taken up at a speed of 183 m/min (600 ft/min) at a position 4 m (13.3 ft) below the spinneret. The filaments passed through the sleeves shown in Figure 3. Seven sleeves were heated to (from top to bottom) 187, 199, 192, 129, 103, 104, and 110°C. No forced flow of air was used, and at a steady state the air temperature at the middle of sleeve was (from top to bottom) 102, 83, 76, 56, 47, 45, and 38°C.

In Figure 4, it is seen that the diameter measured fluctuated within a certain range.

The digital simulation provides a fairly smooth interpolation of the temperature and diameter profiles. The contact null point method for the filament temperature measurement could not be used effectively at the temperature near and above 200°C because the filaments stuck to the temperature probe. Although the spinway height was about 400 cm, the filament diameter leveled off at about 80 cm from the spinneret.

From the data of $T(z)$ and $D(z)$, the real time history of $T(t)$ and $dV(t)/dz$ can be generated by simple coordinate transformation of eq. (5) and by converting D to V.

Example of the Real Time History of Filament Temperature and Rate of Elongation

Figure 5 shows examples of the real time history of temperature and elongation rate which were calculated from the results of interpolation of experimental data. This is for the case of extruding 22.5 g/min of nylon 6 through a 14–10-mil-

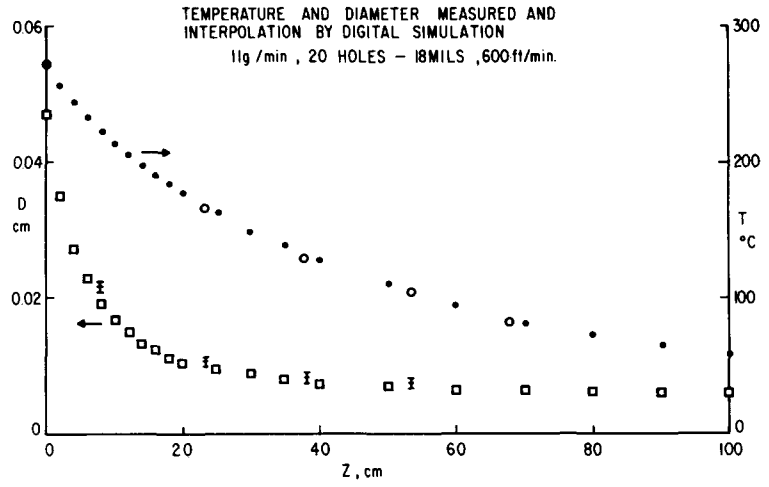

Fig. 4. Temperature and diameter measured and from interpolation by digital simulation: (○) temperature measured; (●) temperature from simulation; (□) diameter from simulation; (∓) diameter measured (indicates range of fluctuation).

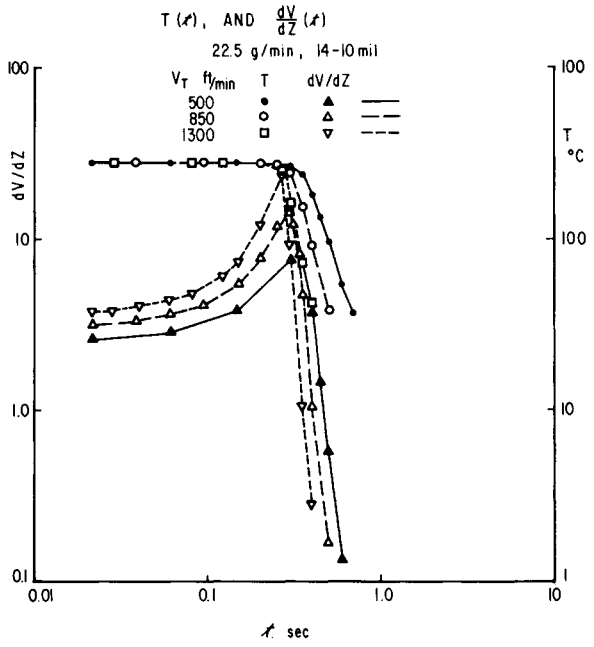

Fig. 5. $T(t)$ and $dV/dz(t)$.

diam-hole spinneret die. While varying the take-up speeds to 152, 259, 396 m/min (500, 850, and 1300 ft/min), the sleeve temperatures were varied so that at each take-up speed maximum tensile strength after drawing was achieved. The drawing was carried out to a fixed draw ratio of 5.3 at one step over a heating block at 180°C.

It is seen in Figure 5 that the temperature history and elongational rate history varied considerably with the variation of the take-up speed. As the take-up speed was increased, the temperature fell faster and the elongational rate was higher to start with, but once it reached maximum point, it also fell faster.

With the differences in the temperature history and the elongational rate history between the three runs, the properties of the spun yarns also show differences. Among these three cases, the case with the take-up speed of 850 ft/min resulted with yarn that gave the highest tensile strength when drawn (11.5 g/denier).

Comparison of the Optimal Runs for Three Different Extrusion Rates

With the spinning system set up as above, the extrusion rate was varied to 22.5, 29.6, and 41.0 g/min, and at each extrusion rate the optimal conditions for maximum tensile strength of the drawn yarn were established by experiments. With these optimal runs for three different extrusion rates, the real time history of temperature and elongation rate were compared in Figure 6.

In this comparison, we observe a striking similarity between the real time histories of the three optimal runs with varying extrusion rates. Although there are slight differences, the points are falling very close to each other. This result confirms the validity of the hypothesis of unique correspondence between the

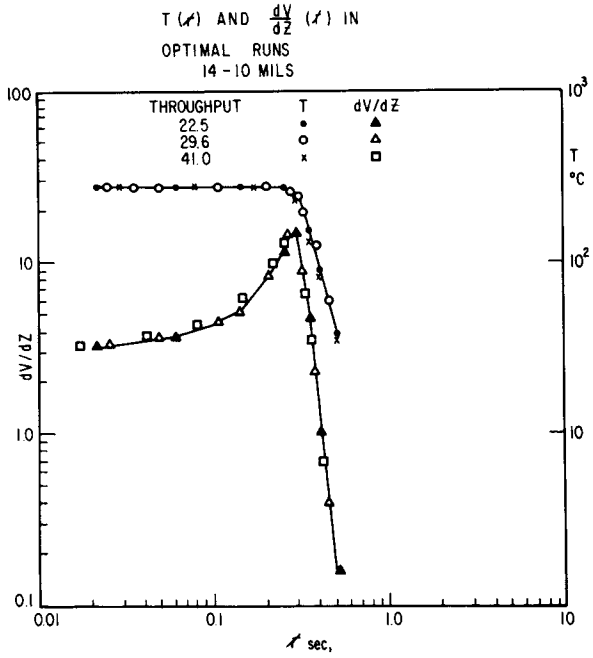

Fig. 6. $T(t)$ and $dV/dz(t)$ in optimal runs.

real time history of temperature and elongational rate and the properties of the spun yarn. Birefringence of the spun yarn was about 0.0025, and the ultimate tensile strength and ultimate elongation of the drawn yarns were 11.5 g/denier and 12% in the three optimal runs.

One interesting feature of this plot shown in Figure 6 is that the temperature history can be characterized roughly by two straight lines. In the plot of elongational rate history, the curve falls almost in a straight line once it goes over the maximum point. The points where the elongational rate is at its maximum value corresponds very closely to the point where the temperature starts falling along the sharp downfall line.

At this time, we are not yet able to offer a clear explanation as to why this particular real time history of the temperature and elongational rate give maximum tensile strength of the drawn yarn. But it is clear that the optimal runs do show similarly in the real time history of the temperature and elongational rate.

Limitations in the Application of the Similarity Criterion of Optimality to Industrial Spinning Processes

A single filament spinning is naturally the simplest case to which application of the above described similarity criterion is easiest. As the number of filaments in the industrial spinning increases, the real time history varies from filament to filament, depending on the position of a particular filament within the bundle of the filaments. This nonuniformity of the real time history of individual filaments translates of course, into the nonuniformity of the properties from

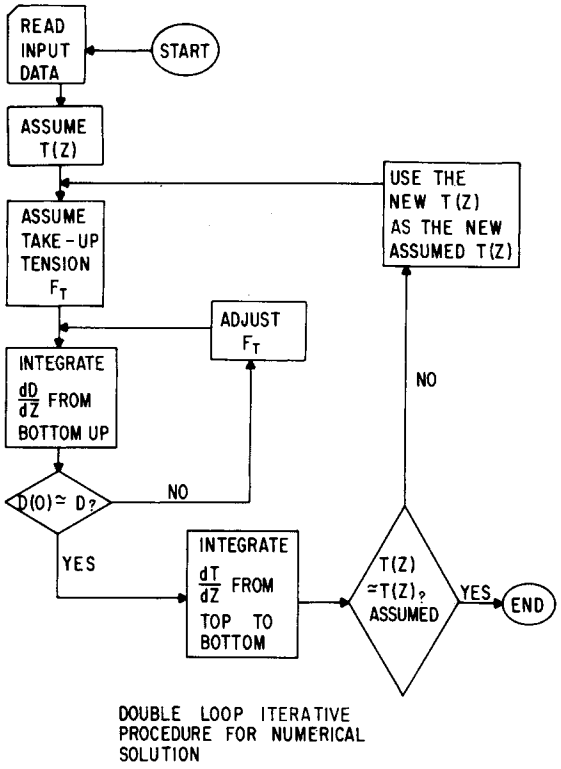

Fig. 7. Double-loop iterative procedure for numerical solution.

filament to filament. As the final property of the yarn product will reflect only the average of these nonuniform filament-to-filament properties, it becomes extremely difficult to realize the improvement achieved with small-scale operation in a large-scale operation.

Nevertheless, the similarity criterion of optimality provides a means of guiding the experimental optimization and scale-up of the spinning process. When properly used, this could help save the cost of optimization and scale-up work of the melt spinning processes.

CONCLUSIONS

From the experimental and simulation studies described in this article the following conclusions can be drawn.

When the melt spinning process is optimized for an objective function with a fiber material on two different rates of extrusion, the real time history of temperature and elongational rate between the two processes is similar. Therefore, this similarity can be used as a criterion in scale-up work in combination with the simulation technique to achieve the scale-up work with less experiments.

APPENDIX A

Digital Simulation of the Melt Spinning Process for the Interpolation of the Data of Temperature and Diameter Measurements

Measurements of filament temperature and filament diameter for an optimized melt spinning can be made only at a limited number of points in the spinway because of the limitations associated with the facilities and operating time. To compare the temperature and diameter profiles of the scaled-up process with those of the original process, we need more number of points of data. So, for the purpose of interpolating the data between the points of measurements, the melt spinning process was simulated on a digital computer.

Digital simulation of the melt spinning process in this case amounts to the iterative numerical solution of eqs. (12) and (19), i.e.,

$$\sigma(z) = \eta_T \frac{dV}{dz} \tag{28a}$$

$$\rho C_p V \frac{dT}{dz} = \frac{-4h_c(T - T_a)}{D} - \frac{4h_r(Tk^4 - T_{sk}{}^4)}{D} \tag{28b}$$

Equation (28a) can be written in terms of the filament diameter by combining with eq. (15) and inserting the mass balance relation of $w = \pi D^2 \rho V/4$,

$$\frac{dD}{dz} = -\frac{\rho F_{\text{rheo}}(z) D(z)}{2w\eta_T} \tag{29}$$

$F_{\text{rheo}}(z)$ is given by eq. (22), and η_T is given by

$$\eta_T = Ae^{B/T}(dV/dz)^{\gamma} \tag{30}$$

in which A, B, and γ are the constants determined by experiments. Value of h_c in eq. (28b) can be estimated by use of eq. (21). The radiative heat transfer coefficient h_r is given by

$$h_r = \alpha \epsilon F_c F_v / \pi \tag{31}$$

where α and ϵ are the Steffan–Boltzmann constant and emissivity, respectively, and F_c and F_v are the geometrical correction factor and view factor which depend on the geometry of the sleeves shown in Figure 3.

In eq. (22), the skin friction owing to air drag τ is a term which is perhaps the most difficult to estimate. This air drag effect was investigated in depth by the present authors.[13] The skin friction τ is approximated by

$$\tau = c_f \rho_a U_f{}^2/2 \tag{32}$$

where c_f is the friction factor and U_f is the filament velocity relative to the air. c_f is approximated by

$$c_f = \frac{4\lambda}{R_{ea}}\left[\frac{1}{G} + \frac{0.5772}{G^2} + \cdots\right] \tag{33}$$

where

$$\left.\begin{aligned} R_{ea} &= U_f a/\nu_a \\ G &= \ln[4Re_z/(Re_a)^2] \\ R_{ez} &= U_f z/\nu_a \end{aligned}\right\} \tag{34}$$

In eq. (34) a and ν_a are the filament radius and kinematic viscosity of the air. The coefficient λ of eq. (33) is a correction factor for the effect of filament swaying in the spinway, and it is a function of the overall drag coefficient.[13]

The pertinent boundary conditions for eqs. (28b) and (29) are

$$\begin{aligned} T(0) &= T_d \\ D(0) &= D_i \\ D(H) &= D_f \end{aligned} \tag{35}$$

where T_d is the die temperature, D_i is the initial filament diameter, and D_f is the take-up diameter. Thus, the diameter is specified at the beginning and end, making it a two-point boundary value problem. Also, we do not know the take-up tension a priori. Because of this nature of the equations and the boundary conditions, the simultaneous solutions of eqs. (28b) and (29) require a double-loop iteration procedure, which is illustrated in Fig. 7.

When the numerical solutions are obtained for $T(z)$ and $D(z)$, they are compared with the experimentally measured data. If the $T(z)$ and $D(z)$ from the simulation match the experimental points well, then we convert the profiles of $T(z)$ and $D(z)$ into $T(t)$ and $dV(t)/dt$. If there is a large discrepancy, the tensile viscosity coefficients, heat transfer coefficients, and air drag coefficients are reviewed and adjusted in such directions that the matching is improved.

Figure 4 shows an example of the comparison of the temperature profile and diameter profile measured with those which resulted from the simulation. It has been found that the iterative scheme of Figure 7 gives a fast-converging solution when a suitable strategy of adjusting the value of F_T is adopted.

References

1. A. Ziabicki, *Kolloid Z.*, **175,** 14 (1961).
2. R. M. Griffith, *Ind. Eng. Chem. Fundam.*, **3**(3), 245 (1964).
3. S. Kase and T. Matsuo, *J. Polym. Sci., Part A* **3,** 2541 (1965).
4. C. D. Han and Y. W. Kim, *J. Appl. Polym. Sci.*, **18,** 2589 (1974).
5. A. Prastaro and P. Parrini, *Text. Res. J.*, **45**(2), 118 (1975).
6. V. G. Bankar, J. E. Spruiell, and J. L. White, *J. Appl. Polym. Sci.*, **21,** 2341 (1977).
7. K. Fujioka and S. Nishiumi, *Kobunshi Kagaku,* **27,** (297), 47 (1970).
8. T. Ishibashi, K. Aoki, and T. Ishii, *J. Appl. Polym. Sci.*, **14,** 1597 (1970).
9. R. R. Lamonte and C. D. Han, *J. Appl. Polym. Sci.*, **16,** 3285 (1972).
10. A. C. Mueller, *Trans. AIChE,* **38,** 613 (1942).
11. L. S. Pontryagin, V. Boltyanski, R. Gamkrelidze and E. Mischchenko, *The Mathematical Theory of Optimal Processes,* Interscience, New York, 1962.
12. Y. D. Kwon and D. C. Prevorsek, unpublished report at Allied Corporation, 1971.
13. Y. D. Kwon and D. C. Prevorsek, *J. Appl. Polym. Sci.*, **23,** 3105 (1979).

Received September 13, 1979
Revised November 30, 1979